Zeitschrift: IABSE publications = Mémoires AIPC = IVBH Abhandlungen
Band: 35 (1975)

Artikel: Trapezoidal bar cells in plane stress
Autor: Hrennikoff, A. / Agrawal, K.M.
DOI: https://doi.org/10.5169/seals-26932

Trapezoidal Bar Cells in Plane Stress

Eléments en forme trapézoïdale chargés dans leur plan

In ihrer Ebene belastete trapezoidale Stabelemente

A. HRENNIKOFF Sc.D.
Research Professor Emeritus of Civil Engineering
University of British Columbia, Vancouver, B.C.
Canada

K.M. AGRAWAL Ph.D.
Research Officer, B.C. Research, Vancouver,
B.C. Canada

General

In solution of plane stress problems by the finite element method trapezoidal cells have advantage over cells of other shapes when the geometry of the plates under investigation may be conveniently described in polar coordinates. In general two quite distinct kinds of cells (elements) are possible, the bar or framework cells and the no-bar cells. The cell proposed here is of the bar type, and it has the shape of an isosceles trapezoid endowed with certain distinctive features contributing to precision. The present study includes the description of the cell and the derivation of its stiffness matrix in explicit form. This is followed by description of results of application of the theory to examples.

Bar Cells

The bar cells used in plane stress problems are made of certain combinations of elastic bars endowed with extensional stiffnesses assuring the same deformability of the model as of the prototype in conditions of any arbitrary uniform stress. The requirement of this equivalence of deformations may be most conveniently satisfied, if the cell is made to deform identically with the plate in the following three separate strain conditions: uniform normal strain ε_x, uniform normal strain ε_y and uniform shearing strain γ_{xy}. The deformations of the cell are judged by the displacements of its corners [2].

The extensional bar stiffnesses EA, found from these relations, on the assumption of the modulus of elasticity E being the same as in the plate, depend on the geometry of the cell and the value of the Poisson's ratio μ of the material of the plate.

In most cases some bar areas become negative within certain ranges of μ and proportions of the cell, and this at times results in lowering of precision. A bar

area may sometimes also become zero. This in effect removes the bar from the cell, making the model in some cases non-rigid and unusable for analysis. The undesirable bar arrangement of this kind may be avoided by the use of additional bars and other special measures.

With the necessary cell geometry decided upon and the bar areas known, the stiffness matrix of the cell is determined.

In analysis of bar stresses in the cell the equations of equilibrium are written for an undeformed structure, on the assumption that the deformations of the bars do not affect appreciably the geometry of the model. Instability of particular bars or groups of bars need not be contemplated.

In the model of the plate the cells of the chosen pattern join each other at the main corners, outlining the shape of the cell. These joints may be considered as hinges, although such articulation is not essential, since the bars are devoid of flexural stiffness. Secondary junctions between the bars belonging to one cell only, are also possible. These joints lie sometimes outside the outline of the particular cell, as will be illustrated presently.

Trapezoidal Bar Cells

The shape of an isosceles trapezoid modelled by the cell is shown in Fig. 1. It is described by the ratios k and k_1 of the two bases and the height of the cell. The thickness of the plate is t.

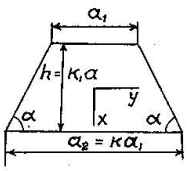

Fig. 1

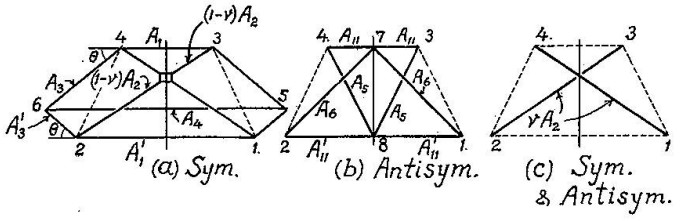

Fig. 2

$$k = \frac{a_2}{a_1} \text{ and } k_1 = \frac{h}{a_1} \tag{1}$$

The bar framework of the cell is presented in Figs. 2a, b and c, depicting a single cell. It consists of several bars, whose cross-section areas are designated by the letters A with different number indices. The areas of the top and bottom bars A_1 and A_1' in Fig. 2a are assumed equal, and so are the areas of the bars A_{11} and A_{11}' in Fig. 2b. The sloping bars A_3 and A_3' are inclined at the same angle θ to the horizontal, and are also equal in areas. The area of the horizontal bar A_4, joining the points 5 and 6, is assumed for simplicity infinite. The bars A_{11} go over the bar A_1 and have common joints 3 and 4 with it, but their intermediate joint 7 is separate from the bar A_1. The bottom bars A_{11}' and A_1' are in a similar situation.

The pairs of nodes 2-3 and 1-4 are joined by two sets of bars, the solid bars in Fig. 2c and the ones in Fig. 2a, attached to each other in a special way at the intersection, by means of a hinged rectangle of infinitesimal size. When the cell is under the action of a loading symmetrical about the vertical axis, the diagonals

2-3 and 1-4 are stressed equally, and the rectangle is fully capable of transmitting their stresses through it, as if it were absent. On the other hand, antisymmetrical loading of the cell would tend to make the stresses in the diagonals equal and opposite in sign; the rectangle would not permit this, and the diagonals would be inactive. In arriving at these conclusions it is necessary to view the cell geometry as undeformed by stress. The area of the solid diagonal bar is assumed νA_2, and of the hinged part $(1-\nu)A_2$, where ν is a fractional coefficient. Thus, the effective area of the diagonal is A_2 under the symmetric loading, and νA_2 under the antisymmetric.

The nodes 1, 2, 3 and 4 are the external joints, at which the cell connects to its neighbours, and where it is acted upon by the external loads. The joints 5 and 6, where the bars A_3, A'_3 and A_4 meet, are parts of the internal mechanism of the cell, unattached to the other cells. With the angles θ as shown, the nodes 5 and 6 protrude into the areas of the neighbouring cells; however, the action of these bars is considered unaffected by such interpenetration.

Simple static analysis shows, that the bars A_3, A'_3 and A_4 are inactive, when the loads are antisymmetric about the vertical axis of symmetry of the cell. At the same time the inclined bars A_5 and A_6 in Fig. 2b are inactive when the loads are symmetrical about the same axis. In case of symmetrical loading the bars A_{11} and A'_{11} become combined with A_1 and A'_1 respectively, and work together with them. The inclined bars νA_2 (Fig. 2c) and the horizontal bars A_{11} and A'_{11} are the only ones which work both under the symmetrical and the antisymmetrical loads.

The cell possesses two free parameters, to be assigned by special considerations, as explained later, the fractional coefficient ν of the diagonal bars and the angle θ of inclination of the side bars A_3 and A'_3. This angle may exceed 90°.

The number of bars in the cell is more than sufficient for its rigidity, even when the values of the parameters k, k_1 and θ combine to make some of the bar areas zero, in other words, cause these bars to disappear.

The uniform strain conditions in the plate ε_x, ε_y and γ_{xy}, which the cell must imitate, are illustrated in Figs. 3a, b and c, with the deformations of the cell indicated by dotted lines. The corner forces X and Y, stated in Fig. 3, are found by transferring the stresses, acting on the edges of the cell, to the corners on the sides of each edge, the transfer being carried out in accordance with statics. In each of the three conditions these corner forces are equal at all corners. It may be observed, that the stress conditions represented in Figs. 3a and b are symmetrical, and the one in Fig. 3c antisymmetrical about the vertical axis x.

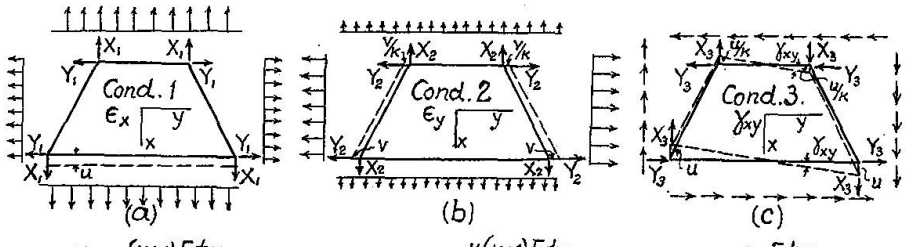

$$X_1 = \frac{(\kappa+1)Et_1u}{4\kappa_1(1-\mu^2)} \qquad Y_1 = \frac{\mu Et_1u}{2(1-\mu^2)}$$

$$X_2 = \frac{\mu(\kappa+1)Et_1v}{2\kappa(1-\mu^2)} \qquad Y_2 = \frac{\kappa_1 Et_1v}{\kappa(1-\mu^2)}$$

$$X_3 = \frac{\kappa_1 Et_1u}{2\kappa(1+\mu)} \qquad Y_3 = \frac{(\kappa+1)Et_1u}{4\kappa(1+\mu)}$$

Fig. 3

Determination of the Bar Areas

The cell of Fig. 2 is subjected to the strain Condition 1, uniform strain in x direction, Fig. 3a. The four corners develop the forces X_1 and Y_1, as shown. The antisymmetrical bars A_5 and A_6 of Fig. 2b remain idle. The stresses in the bars A_3 and A_3' are equal, in view of equality of their angles of inclination to horizontal. The stresses F_2 and F_3 in the bars A_2 and A_3 may be expressed in terms of the geometry of the cell, the elongation u and the areas of the bars. Equating the sums of the x and y components of F_2 and F_3 to the nodal forces X_1 and Y_1 in Fig. 3a, the areas A_2 and A_3 are found as follows

$$A_2 = \frac{[(k+1)+2\mu k_1 \tan\theta]\,[4k_1^2+(k+1)^2]^{3/2}}{16k_1^2(1-\mu^2)\,2k_1+(k+1)\tan\theta}\,a_1 t. \tag{2}$$

$$A_3 = \frac{[(k+1)^2-4\mu k_1^2]}{4(1-\mu^2)\,[2k_1\cos\theta+(k+1)\sin\theta]\sin^2\theta}\,a_1 t. \tag{3}$$

The cell is now strained horizontally in accordance with the Condition 2 in Fig. 3b. The bars $(A_1 + A_{11})$ and $(A_1' + A_{11}')$ are stressed equally in view of equality of their areas and proportionality of elongations to their lengths. The bars of Fig. 2b, other than A_{11} and A_{11}' again develop no stress. Following a procedure similar to the one just outlined, the equation $\sum Y = 0$ at one of the corners of the cell leads to determination of the stress F_1 in the top and bottom horizontal bars and to the expression for the sum of the areas $(A_1 + A_{11})$.

$$(A_1 + A_{11}) = \frac{(k+1)\,[4\mu k_1^2-(k+1)^2]+2k_1\tan\theta\,[4k_1^2-\mu(k+1)^2]}{16k_1^2(1-\mu^2)\tan\theta}\,a_1 t \tag{4}$$

It may be pointed out that the equation $\sum X = 0$ can give no new information, being satisfied automatically by Betti's reciprocal theorem, irrespective of the areas of bars.

The shear Condition 3 (Fig. 3c) causes stresses in the antisymmetric system of bars of Fig. 2b with participation of the diagonals νA_2. The ratio of components of corner forces in Condition 3 is

$$\frac{X_3}{Y_3} = \frac{2k_1}{k+1} \tag{5}$$

This indicates, that the resultants of X_3 and Y_3 at all corners act in the directions of the diagonals.

For purposes becoming clear later, it is desirable to subdivide the corner forces X_3 and Y_3 into parts carried by the diagonals νA_2 and the antisymmetrical bar system of Fig. 2b. These parts, expressed in terms of a new fractional parameter η, are presented in Figs. 4a and b. By equating the stress in the diagonal in Fig. 4b to its expression in terms of the elongation of the bar νA_2, the parameter η is found related to ν by the equation

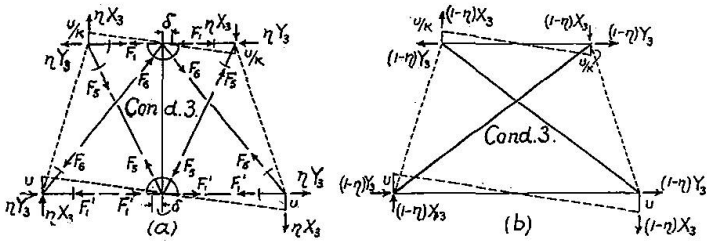

Fig. 4

$$(1-\eta)=\nu\frac{(k+1)\left[(k+1)+2\mu k_1\tan\theta\right]}{k_1(1-\mu)\left[2k_1+(k+1)\tan\theta\right]} \tag{6}$$

The antisymmetrically loaded structure of Fig. 4a is statically determinate, and the stresses in all its bars, equal and opposite in sign on the opposite sides of the axis of symmetry, are expressible in terms of the corner forces. Thus the stresses in the horizontal members are

$$\left.\begin{aligned} F_1&=\frac{k}{2k_1}X_3=\frac{k}{k+1}\eta Y_3\\ F_1'&=\frac{1}{2k_1}X_3=\frac{1}{k+1}\eta Y_3\end{aligned}\right\} \tag{7}$$

The areas of these bars could be found in terms of the displacement u and the geometry of the cell, but this is not needed for determination of the terms of the stiffness matrix.

The bar systems pictured in Figs. 4a and b provide two independent alternative routes for the corner forces X_3 and Y_3 to travel through the cell. For this reason the parameter η must be viewed at this stage as an arbitrary number of a magnitude anywhere between zero and unity.

Terms of the Stiffness Matrix

Condition u_1

If the bar areas in the cell are known, the nodal forces in it, produced by unit displacements of any of the nodes, such as $u_1=1$, may be found using the equations of structural theory. This however is a laborious procedure, and in many cases it is possible to arrive at the same results more easily by a judicial combination of several elementary strain conditions with knowledge of only a few bar areas, and even without them. In the present case of the trapezoidal bar cell the method of combination of elementary conditions also leads to a significant refinement of the cell, resulting in improvement of precision. The combination producing the Condition $u_1=1$, is presented in Fig. 5.

The three component conditions are the basic Conditions 1 and 3, and a non-basic flexural Condition 4, in which the nodes move in x direction. The corner

displacements in these three conditions add up to zero, except for the corner 1, where their sum equals u_1. The corner forces in Fig. 5, on comparison with those in Fig. 3, are one half as great for the Condition 1 and one quarter as great for the Condition 3.

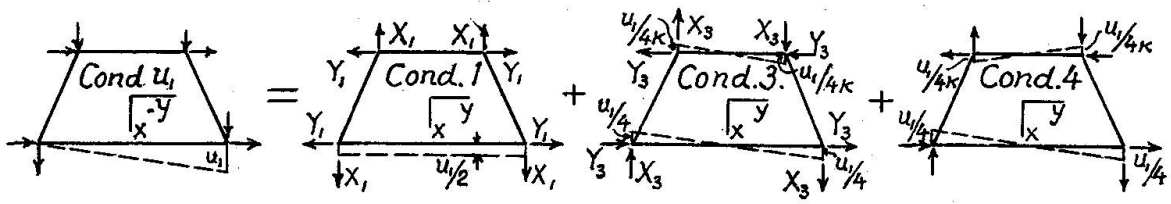

Fig. 5

The Condition 4, as the Condition 3, is antisymmetrical, and its corner forces may be deduced from comparison of its corner displacements with those in Condition 3. For this purpose Condition 4 is broken up into two parts, shown in Figs. 6a and b, corresponding to separate actions of the diagonals and the antisymmetric bar system.

As follows from comparison of corner displacements, the diagonal bars in Fig. 6b deform less than in Fig. 4b in the ratio $\frac{k-1}{k+1}$, and so the components of their stresses must stand in the same ratio.

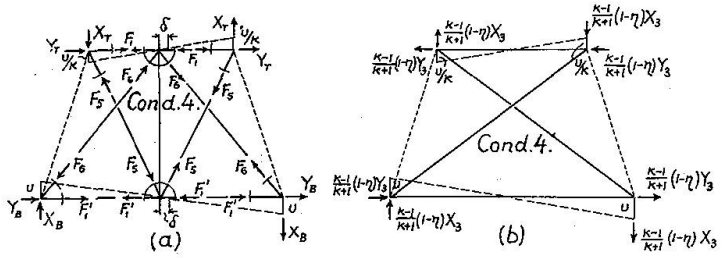

Fig. 6

$$\text{Thus, } X = \frac{k-1}{k+1}(1-\eta)X_3 \text{ and } Y = \frac{k-1}{k+1}(1-\eta)\,Y_3 \tag{8}$$

The corner displacements of the antisymmetrical bar system in Fig. 6a equal those in Fig. 4a, and so must do the horizontal displacements of the junctions of the horizontal and the inclined bars, in order to preserve the equilibrium between the horizontal and the inclined members. For this reason all bar stresses in Fig. 6a are numerically equal to those in Fig. 4a, although their signs, as indicated by arrows in both figures, are in some members different.

The corner forces in Fig. 6a may now be expressed by comparison with Fig. 4a, making use of Eqs. (7).

$$\left.\begin{aligned} X_B &= X_T = \eta X_3 \\ Y_B &= \eta Y_3 - 2F_1' = \frac{k-1}{k+1}\eta Y_3 \\ Y_T &= \eta Y_3 - 2F_1 = -\frac{k-1}{k+1}\eta Y_3 \end{aligned}\right\} \tag{9}$$

Combining these with the ones in Fig. 6b, the total corner forces in the Condition 4 (see Fig. 7) are:

$$\left.\begin{aligned} X_{4B} &= \frac{k-1}{k+1}X_3 + \frac{2}{k+1}\eta X_3 \\ X_{4T} &= \frac{k-1}{k+1}X_3 - \frac{2k}{k+1}\eta X_3 \\ Y_{4B} &= Y_{4T} = \frac{k-1}{k+1}Y_3 \end{aligned}\right\} \tag{10}$$

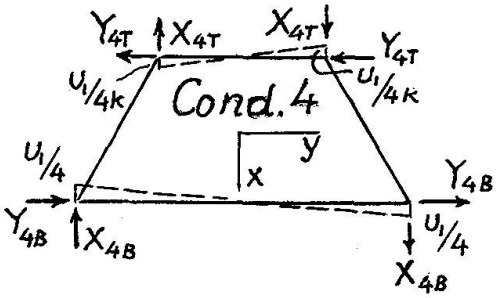

Fig. 7

The members of the first column of the stiffness matrix of the cell, i.e. the corner forces corresponding to Condition $u_1 = 1$, are found by adding up the values of the three component cases in Fig. 5, and are stated in Table 1.

Condition v_1

This condition may likewise be obtained by addition of the three component conditions, the basic Conditions 2 and 3, and the non-basic flexural Condition 5, in which the strains occur in y direction (Fig. 8).

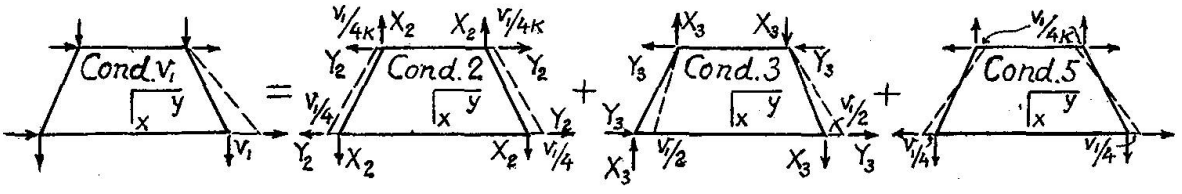

Fig. 8

Table 1. Trapezoidal Bar Cell

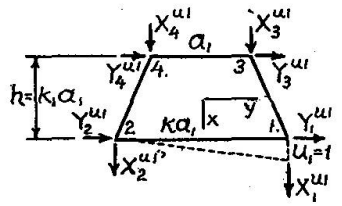

$$X_1^{u1} = \left[\frac{(k+1)^2 + 2k_1^2(1-\mu) + 2\frac{\eta}{k}k_1^2(1-\mu)}{8(k+1)k_1(1-\mu^2)}\right] Et$$

$$X_2^{u1} = \left[\frac{(k+1)^2 - 2k_1^2(1-\mu) - 2\frac{\eta}{k}k_1^2(1-\mu)}{8(k+1)k_1(1-\mu^2)}\right] Et$$

$$X_3^{u1} = \left[\frac{-(k+1)^2 + 2k_1^2(1-\mu) - 2\eta k_1^2(1-\mu)}{8(k+1)k_1(1-\mu^2)}\right] Et$$

$$X_4^{u1} = \left[\frac{-(k+1)^2 - 2k_1^2(1-\mu) + 2\eta k_1^2(1-\mu)}{8(k+1)k_1(1-\mu^2)}\right] Et$$

$$Y_1^{u1} = -Y_4^{u1} = \frac{Et}{8(1-\mu)}$$

$$Y_2^{u1} = -Y_3^{u1} = \frac{1-3\mu}{8(1-\mu^2)} Et$$

Table 2. Trapezoidal Bar Cell

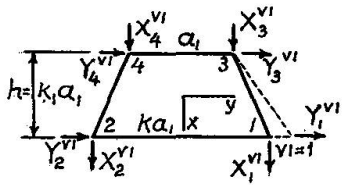

$$Y_1^{v1} = \frac{8k_1^2 + (k+1)^2(1-\mu) + 16\frac{A_1 + A_{11}}{kat}k_1(1-\mu^2)}{16(k+1)k_1(1-\mu^2)} Et$$

$$Y_2^{v1} = \frac{-8k_1^2 + (k+1)^2(1-\mu) - 16\frac{A_1 + A_{11}}{kat}k_1(1-\mu^2)}{16(k+1)k_1(1-\mu^2)} Et$$

$$Y_3^{v1} = \frac{8k_1^2 - (k+1)^2(1-\mu) - 16\frac{A_1 + A_{11}}{at}k_1(1-\mu^2)}{16(k+1)k_1(1-\mu^2)} Et$$

$$Y_4^{v1} = \frac{-8k_1^2 - (k+1)^2(1-\mu) + 16\frac{A_1 + A_{11}}{at}k_1(1-\mu^2)}{16(k+1)k_1(1-\mu^2)} Et$$

$$X_1^{v1} = -X_4^{v1} = \frac{Et}{8(1-\mu)}$$

$$X_3^{v1} = -X_2^{v1} = \frac{(1-3\mu)}{8(1-\mu^2)} Et$$

The nodal forces of the flexural Condition 5 may be correlated with those of Condition 2 by observing the displacements of the joints and the action of the bars forming the cell (Fig. 9). Since both Conditions 2 and 5 are symmetrical about the vertical axis, the bars A_5 and A_6 are inactive.

The horizontal movements of the nodes 1 and 2 are both outward and equal to $\frac{v_1}{4}$, while the displacements of the upper nodes $\frac{v_1}{4k}$ are outward in Condition 2 and inward in Condition 5.

The nodal forces in both conditions are contributed by the inclined bars A_2, A_3 and A_3', and the double horizontal bars $(A_1 + A_{11})$ and $(A_1' + A_{11}')$. The stresses in the inclined bars, and the nodal forces resulting from them, stand in the ratio of the algebraic sums of their nodal displacements, i.e. in the ratio $\frac{k-1}{k+1}$.

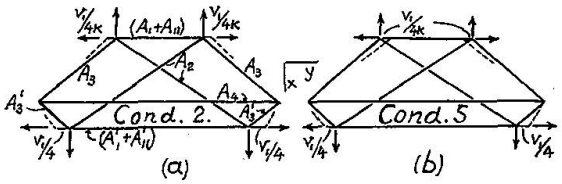

Fig. 9

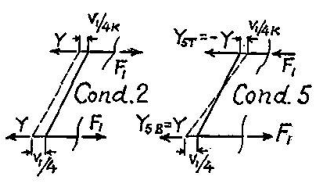

Fig. 10

The stresses F_1 are numerically equal in all horizontal bars in both conditions 2 and 5. In the first of these, F_1 are tensile, and in the second – tensile at the bottom and compressive at the top, as indicated in Fig. 10. Their contributions, Y_{5B} at the bottom, and Y_{5T} at the top, to the horizontal nodal forces may be expressed as follows:

$$Y_{5B} = F_1 = \frac{k-1}{k+1} F_1 + \frac{2}{k+1} F_1$$

and $$Y_{5T} = -F_1 = \frac{k-1}{k+1} F_1 - \frac{2k}{k+1} F_1.$$

The first parts of these expressions may be combined with the contributions of the other bars, and the total nodal forces in Condition 5 may be expressed through their counterparts in Condition 2 and the stresses F_1 as follows:

$$\begin{aligned} X_5 &= \frac{k-1}{k+1} X_2 \\ Y_5 \text{ (bot. joints)} &= \frac{k-1}{k+1} Y_2 + \frac{2}{k+1} F_1 \\ Y_5 \text{ (top joints)} &= \frac{k-1}{k+1} Y_2 - \frac{2k}{k+1} F_1 \end{aligned} \tag{11}$$

The corner forces X_2 and Y_2 of these expressions are given in Fig. 8. The forces F_1 are:

$$F_1 = \frac{(A_1 + A_{11})\, E v_1}{2k a_1} \tag{12}$$

The terms of the second column of stiffness matrix, corresponding to the Condition $v_1 = 1$, are stated in Table 2.

Other Terms of the Stiffness Matrix

The matrix terms, produced by the displacements of the node 3, are found by procedures similar to the ones described, and those corresponding to the displacements of the nodes 2 and 4, by applying the principles of symmetry to the terms already found.

Refinement of the Stiffness Matrix

The desired stiffness matrix should be applicable to isosceles trapezoids of all kinds, including rectangles, whose coefficient $k = 1$.

While the matrix of Tables 1 and 2 describes stresses and strains in uniform strain conditions perfectly, its descriptions of non-uniform conditions naturally is

only approximate. Furthermore, the arrangement of framework in a rectangular cell, viewed as a special case of a trapezoid, is different in x and y directions, and so it may be expected, that the results of analyses of model made of such cells, would depend on orientation of rectangles, with some unfavourable effect on precision, which is likely to extend to cells with values of k distinct from unity. Experience confirms correctness of this supposition.

Fortunately however, the existence of free parameters θ and ν or η makes possible a refinement of the stiffness matrix with favourable effect on precision. The idea is to assign to θ and ν such values, that the limiting case of a trapezoid with $k = 1$ will have the same elastic properties in the directions of both axes.

The terms X^{u1} and Y^{v1} of the stiffness matrix in Tables 1 and 2 involve quantities η and $(A_1 + A_{11})$. These are present only in the last members of the numerators of their expressions. Replace these members by different expressions involving a new parameter ω. This version of the stiffness matrix is assembled in Table 3. The parameter ω in it is related to η and $(A_1 + A_{11})$ by the expressions

$$\omega = \frac{\eta k_1^2 (1-\mu)}{2} = \frac{2(A_1 + A_{11})(1-\mu^2)}{k_1 a_1 t} \tag{13}$$

On substitution of $k = 1$ in Table 3 the terms X_1^{u1} and Y_1^{v1} (see Fig. 11) become

$$\left.\begin{aligned} X_1^{u1} &= \frac{2 + k_1^2 (1-\mu) + 2\omega}{8k_1 (1-\mu^2)} \\ Y_1^{v1} &= \frac{2k_1^2 + 1 - \mu + 2k_1^2 \omega}{8k_1 (1-\mu^2)} \end{aligned}\right\} \tag{14}$$

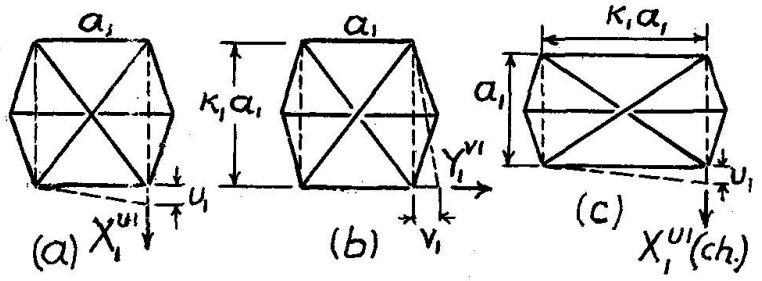

Fig. 11

It may be pointed out, that introduction of the new parameter ω is legitimate. This is simply equivalent to attributing some particular values to the quantity η and the angle θ. ω as η must be positive.

Change now the bar arrangement from Fig. 11a to Fig. 11c. The new expression for X_1^{u1} is obtainable from the old by replacing k_1 with $\frac{1}{k_1}$. This makes X_1^{u1} (changed) identical with Y_1^{v1} in Eq. (14). Similarly, Y_1^{v1} (changed) is found the same as X_1^{u1}. It may be observed, that the members with ω satisfying Eq. (13), fit all terms of the stiffness matrix, and not just X_1^{u1} and Y_1^{v1}.

Table 3. Trapezoidal Bar Cell

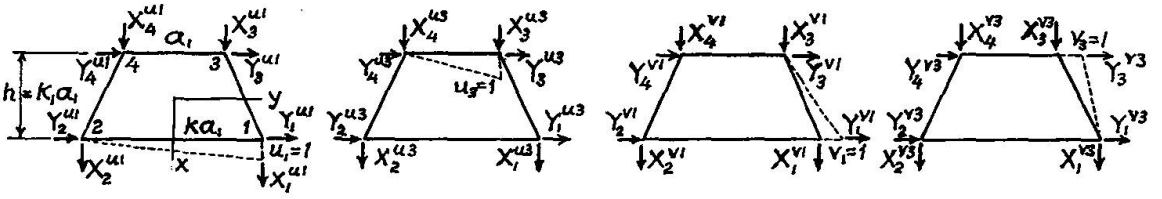

$$X_1^{u1} = \frac{(k+1)^2 + 2k_1^2(1-\mu) + \dfrac{4\omega}{k}}{8k_1(k+1)(1-\mu^2)} Et$$

$$X_2^{u1} = \frac{(k+1)^2 + 2k_1^2(1-\mu) + \dfrac{4\omega}{k}}{8k_1(k+1)(1-\mu^2)} Et$$

$$X_3^{u1} = \frac{-(k+1)^2 + 2k_1^2(1-\mu) - 4\omega}{8k_1(k+1)(1-\mu^2)} Et$$

$$X_4^{u1} = \frac{-(k+1)^2 - 2k_1^2(1-\mu) + 4\omega}{8k_1(k+1)(1-\mu^2)} Et$$

$$X_1^{u3} = \frac{-(k+1)^2 + 2k_1^2(1-\mu) - 4\omega}{8k_1(k+1)(1-\mu^2)} Et$$

$$X_2^{u3} = \frac{-(k+1)^2 - 2k_1^2(1-\mu) + 4\omega}{8k_1(k+1)(1-\mu^2)} Et$$

$$X_3^{u3} = \frac{(k+1)^2 + 2k_1^2(1-\mu) + 4k\omega}{8k_1(k+1)(1-\mu^2)} Et$$

$$X_4^{u3} = \frac{(k+1)^2 - 2k_1^2(1-\mu) - 4k\omega}{8k_1(k+1)(1-\mu^2)} Et$$

$$X_1^{v1} = \frac{1}{8(1-\mu)} Et$$

$$X_2^{v1} = -\frac{1-3\mu}{8(1-\mu^2)} Et$$

$$X_3^{v1} = \frac{1-3\mu}{8(1-\mu^2)} Et$$

$$X_4^{v1} = -\frac{1}{8(1-\mu)} Et$$

$$X_1^{v3} = -\frac{1-3\mu}{8(1-\mu^2)} Et$$

$$X_2^{v3} = \frac{1}{8(1-\mu)} Et$$

$$X_3^{v3} = -\frac{1}{8(1-\mu)} Et$$

$$X_4^{v3} = \frac{1-3\mu}{8(1-\mu^2)} Et$$

$$Y_1^{u1} = \frac{1}{8(1-\mu)} Et$$

$$Y_2^{u1} = \frac{1-3\mu}{8(1-\mu^2)} Et$$

$$Y_3^{u1} = -\frac{1-3\mu}{8(1-\mu^2)} Et$$

$$Y_4^{u1} = -\frac{1}{8(1-\mu)} Et$$

$$Y_1^{u3} = \frac{1-3\mu}{8(1-\mu^2)} Et$$

$$Y_2^{u3} = \frac{1}{8(1-\mu)} Et$$

$$Y_3^{u3} = -\frac{1}{8(1-\mu)} Et$$

$$Y_4^{u3} = -\frac{1-3\mu}{8(1-\mu^2)} Et$$

$$Y_1^{v1} = \frac{8k_1^2 k + k(k+1)^2(1-\mu) + 8k_1^2\omega}{16k(k+1)k_1(1-\mu^2)} Et$$

$$Y_2^{v1} = \frac{-8k_1^2 k + k(k+1)^2(1-\mu) - 8k_1^2\omega}{16k(k+1)k_1(1-\mu^2)} Et$$

$$Y_3^{v1} = \frac{8k_1^2 - (k+1)^2(1-\mu) - 8k_1^2\omega}{16(k+1)k_1(1-\mu^2)} Et$$

$$Y_4^{v1} = \frac{-8k_1^2 - (k+1)^2(1-\mu) + 8k_1^2\omega}{16(k+1)k_1(1-\mu^2)} Et$$

$$Y_1^{v3} = \frac{8k_1^2 - (k+1)^2(1-\mu) - 8k_1^2\omega}{16(k+1)k_1(1-\mu^2)} Et$$

$$Y_2^{v3} = \frac{-8k_1^2 - (k+1)^2(1-\mu) + 8k_1^2\omega}{16(k+1)k_1(1-\mu^2)} Et$$

$$Y_3^{v3} = \frac{8k_1^2 + (k+1)^2(1-\mu) + 8kk_1^2\omega}{16(k+1)k_1(1-\mu^2)} Et$$

$$Y_4^{v3} = \frac{-8k_1^2 + (k+1)^2(1-\mu) - 8kk_1^2\omega}{16(k+1)k_1(1-\mu^2)} Et$$

The Value of ω

The question of what values of ω should be preferably assigned to the cells composing the model may be answered by resorting to the energy principles.

Suppose, that by using some particular values of this parameter the nodal displacements of all cells in the model, under the action of given loads, have been determined. Consider one of these cells by itself, and apply to it the three uniform strain conditions in appropriate amounts, so that the nodes 2, 3 and 4 are placed in their relative positions conforming to the distortion of the model, while the node 1 still remains short of its proper place. The cell so deformed is held in this state by appropriate nodal forces, none of which is a function of the parameter ω. To make the node 1 move the remaining distances u_o and v_o (Fig. 12), it is necessary to apply to it additional forces

$$X = X_1^{u1}\, u_o + X_1^{v1}\, v_o$$
$$Y = Y_1^{v1}\, v_o + Y_1^{u1}\, u_o \tag{15}$$

while restraining the other nodes from further movements.

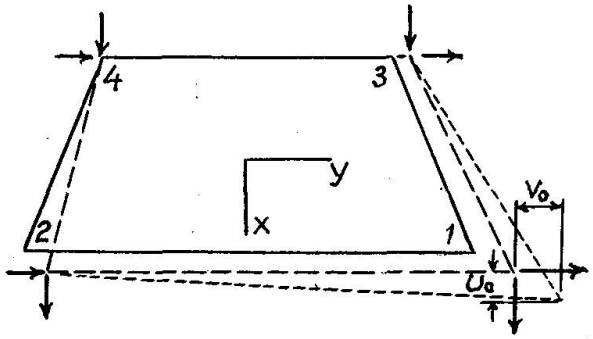

Fig. 12

The forces represented by the first terms in the expressions for X and Y always act in the directions of u_o and v_o, irrespective of the signs of these displacements, thus making positive contributions to the energy of deformation of the cell. The contributions of the second terms to the energy of deformation may be positive or negative, but their effect is minor.

Re-assemble now all cells of the model. The energy of its deformation U is composed of the energies of individual cells. Assume, that ω is decreased, while all nodes are left in the same locations. For this they must be restrained, because the assembly is no more in equilibrium. A smaller ω makes the terms X_1^{u1} and Y_1^{v1}, and with them the energy of deformation U, smaller, while the potential energy of the loads V is the same as before, because the nodes have not moved. This makes the total energy of the system T smaller than before.

Now remove slowly the nodal restraints and allow the model to find its new state of equilibrium. By the Rayleigh-Ritz principle the energies U and V change in such a way, that their sum T decreases. A smaller ω thus has resulted in a smaller T of the deformed structure.

The same reasoning is equally valid in application to models constructed of other types of cells, both bar and no-bar. Cells with smaller values of X_1^{u1} and Y_1^{v1} would possess a smaller total energy T of the model than cells of the same shape and size, but with bigger X_1^{u1} and Y_1^{v1} terms.

A question still remains, which of the two sets of terms X_1^{u1}, Y_1^{v1}, or more generally, what kind of cell, is better for precision of results. This question presents itself, as the cells are subdivided into smaller units, with zero size being the limit, when the model becomes in effect the actual plate prototype.

The numerical progress of energy T on subdivision of cells has been examined closely on models composed of rectangular cells [4]. The value of T on reduction of the size of cells in such models was found to increase or to decrease, at times non-monotonically, with the direction of change depending mostly on the stiffness matrix terms of the cells used. Since rectangle is a special case of trapezoid, one may expect, that with trapezoidal cells the convergence of the total energy should also proceed up or down numerically depending on the particulars of the problem, including the type of cells with their parameters k and k_1, and the geometry of the structure and its loading. These relationships will be demonstrated below on examples.

A few explanatory words about the parameter ω are in order. This parameter should be positive, but not zero. If $\omega = 0$, the antisymmetrical bar system of the cell is eliminated. This feature is not objectionable in itself, but it makes the nodal forces, brought about by unit movements of the nodes 1 and 3, equal at respective corners, which is unreasonable. If $\omega = 0$, a rectangular cell becomes non-rigid.

It is necessary to point out, that negative bar areas, making their appearance in certain geometrical configurations of cells, and leading in some framework systems to reduced precision, need not be feared in case of cells under consideration, because they all become absorbed in a single positive parameter ω.

While solution of a cell model resulting in a better energy T is superior to the ones characterized by less satisfactory values of T, this does not necessarily signify superiority of precision of displacements everywhere in the model. For its equilibrium structure seeks condition of the least total energy. This roughly corresponds to least weighted errors in deflections of the points of application of loads in the directions of the loads. Deflections normal to the loads, as well as the ones of the unloaded nodes, are not reflected in the value of T.

Examples

The application of the theory presented here is illustrated on displacement analysis of a thin plate of thickness t in the shape of a 90° sector of hollow circle (Fig. 13), acted upon by a radial load, applied on one radial edge, while the other edge is supported on rollers, allowing its points to move only radially. An exact solution of this problem is available [5].

In the examples solved here the inner radius is assumed to be one third of the outer radius R. The Poisson's ratio $\mu = 0.2$. The boundary conditions allow the

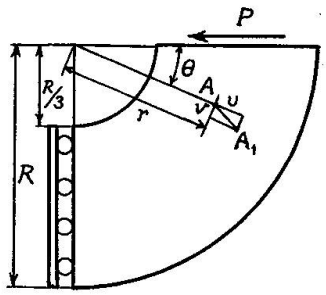

Fig. 13

plate to undergo an arbitrary vertical movement; this in the theoretical solution is assigned a certain definite value. The expressions for the radial and tangential displacements, u and v respectively, are given by Eqs. (16) and (17), in which r and θ signify the polar coordinate of the point.

$$u = \left\{\left[-3.34882\,(1-\mu)\,1n\frac{r}{R} + 1.50697\,(1-3\mu)\,\frac{r^2}{R^2} - 0.16744\,(1+\mu)\,\frac{R^2}{r^2}\right]\sin\theta - \right.$$
$$\left. - 10.5206\cos\theta + 6.69764\,\theta\cos\theta\right\}\frac{P}{Et} \tag{16}$$

$$v = \left\{10.5206\sin\theta - \left[3.34882\left((1+\mu)+(1-\mu)1n\frac{r}{R}\right) + 1.50697\,(5+\mu)\,\frac{r^2}{R^2} - \right.\right.$$
$$\left.\left. - 0.16744\,(1+\mu)\,\frac{R^2}{r^2}\right]\cos\theta - 6.69764\,\theta\sin\theta\right\}\frac{P}{Et} \tag{17}$$

The tangential stress by means of which the load P is applied to the edge $\theta = 0$, is given by the equation

$$\tau_{r\theta} = \left[\frac{3.34882}{r} - \frac{3.01394\,r}{R^2} - \frac{0.33488\,R^2}{r^3}\right]\frac{P}{t}. \tag{18}$$

The finite element models used in solution of this problem are formed by subdividing the plate into trapezoids by radial and circumferential lines. To trace the improvement of precision with reduction of mesh size three models are used. The coarsest one of 15 cells has 3 cells in radial direction and 5 in tangential (Fig. 14). Two other models possess 60 and 240 cells, i.e., two and four times as many cells in each direction as the first model.

To reduce the number of significant variables and by that to simplify the problem of identifying the more precise types of elements, the elements are made geometrically similar in all circumferential rows. Elements so proportioned have the same parameters k and k_1, and the same stiffness matrices in spite of difference in sizes, as they grow larger away from the centre.

Geometry of the cells and the model may be easily determined by elementary means.

The parameter k, which is also the magnification factor between two radially adjacent cells is $k = \sqrt[n]{3}$, where n is the number of circumferential rows, i.e., 3, 6 and 12 in the three models employed.

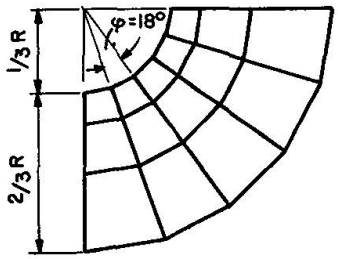

Fig. 14

The parameter $k_1 = \dfrac{k-1}{2 \tan \frac{1}{2}\varphi}$, where φ is the central angle subtended by each cell and equal to 18°, 9° and 4°30′. The small base of the smallest trapezoid $a = 2/3\ R \sin \frac{1}{2}\varphi$.

The numerical values of these quantities are assembled in Table 4.

Table 4. Value of Significant Quantities of Cells in Models Used

Quantity	Model 5 × 3 Cells	10 × 6 Cells	20 × 12 Cells
a_1	0.104290	0.052306	0.026173
k	1.44225	1.200936	1.09587
k_1	1.39613	1.28052	1.22003

The shearing stress $\tau_{r\theta}$ (Eq. 18) on the edge $\theta = 0°$ is non-uniform; this raises question of how to assign proper fractions of the active load P to the nodes on this edge. Fig. 15 shows three consecutive edge nodes A, B, C and their distances from the centre of the sector. It is felt, that a load element dP, situated

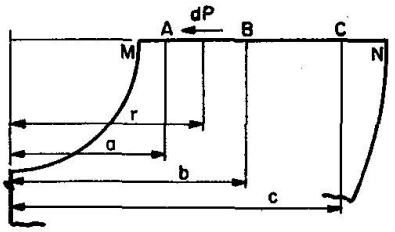

Fig. 15

between the nodes A and B should contribute only to these two nodes, and that its contribution at the node nearer it should be greater than at the more distant one. From these considerations nodal concentrations at B have been determined by "the Law of Proximity", mathematically identical with the law of the lever. This was done separately for the contributions coming from the inner panel AB and the outer panel BC. The extreme nodes M and N have their contributions coming only from one side.

The computed values of the nodal loads in the three models used, numbered from the inside, are stated in Table 5.

Table 5. Nodal Loads in Models Used. Numbered from Inside the Sector

Model 5 × 3 Cells	Model 10 × 6 Cells	Model 20 × 12 Cells	
$P_o = 0.086925\ P$	$P_0 = 0.025530\ P$	$P_0 = 0.006930\ P$	$P_7 = 0.119020\ P$
$P_1 = 0.398441\ P$	$P_1 = 0.135140\ P$	$P_1 = 0.039011\ P$	$P_8 = 0.109722\ P$
$P_2 = 0.411183\ P$	$P_2 = 0.215155\ P$	$P_2 = 0.070124\ P$	$P_9 = 0.093734\ P$
$P_3 = 0.103452\ P$	$P_3 = 0.241144\ P$	$P_3 = 0.093426\ P$	$P_{10} = 0.070608\ P$
	$P_4 = 0.216664\ P$	$P_4 = 0.109595\ P$	$P_{11} = 0.039518\ P$
	$P_5 = 0.138483\ P$	$P_5 = 0.119015\ P$	$P_{12} = 0.007220\ P$
	$P_6 = 0.027883\ P$	$P_6 = 0.122073\ P$	

Finite Element Solution

In view of circular shape of the model the x and y axes of the adjacent cells at the common nodes do not coincide (Fig. 16). Convenience of computer programming calls for the use of nodal displacements in the radial and tangential directions r and t, common to the neighbouring cells.

Fig. 16

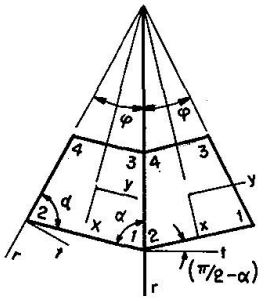

The stiffness matrix of the cell in model coordinates $[K_o]$ is found from the one in cell coordinates $[K]$ by the equation

$$[K_o] = [L]\,[K]\,[L]^T \tag{19}$$

in which $[L]$ is the transformation matrix for the vectors of nodal displacements or forces, from the cell to the model coordinates, and $[L]^T$ is its transpose. Derivation of explicit expressions for the terms of $[K_o]$ is laborious and must be left to computer.

To make nodal displacements in the model solution consistent with the theoretical values, one of its nodes on the edge $\theta = \frac{1}{2}\pi$ must be given the exact value of u in Eq. (16). This calls for an additional step in the solution of the model. As the node in question, in this case the inner node on the edge $\theta = \frac{1}{2}\pi$, is being moved radially to its intended location, the three adjacent nodes, one on the same edge, and two on the neighbouring radial line, are kept at rest. This requires application to these nodes of the load vector equal to the product of proper terms of stiffness matrix and the displacement of the moved node. Following this, the moved node is kept at rest, and the reverse of the load vector at the three neighbouring nodes is added on to the active load system in solving the model for the displacement of the nodes.

Results

Calculation of displacements of the cell nodes in the sector plate is carried out with both, the bar cells described in this work, and the no-bar cells of the same trapezoidal shape [3], using the energy type stiffness matrix.

The action of the plate under consideration is substantially that of a sharply curved short cantilever beam, fixed at one end. Most of movement occurs in radial direction at the loaded free end, and it gets gradually smaller on recession from it. There is also some tangential movement resulting from normal stresses in lengthwise direction, tension on the outside and compression on the inside of the sector.

The bar cells of all three models are endowed with the values of the parameter ω equal to 0.001, 0.02, 0.2, 0.4. No-bar cells are also used.

In Table 6 the nodal displacements, or rather their coefficients c before $\frac{P}{Et}$, determined by the finite element method, are compared with the exact values, given by Eqs. (16) and (17). Quality of each solution is described by the greatest at all nodes value of error in c, separately in radial and tangential displacements. In the same table are also stated the percentages of the total number of nodes, at which the percentage error is no more than 2% in the coarse model, and 1% in the two other models.

To correlate the quality of the obtained displacement values with the total energies T of the deformed models, the values of the latter are stated in the table and also presented graphically in Fig. 17.

Since the true values of u given by Eq. (16) on the radial line $\theta = 0°$, over which the load P is distributed, are all the same and are equal to $10.5206\ \frac{P}{Et}$, the actual total energy of the sector is $T = -\frac{1}{2}(10.5206)\frac{P^2}{Et} = -5.2603\frac{P^2}{Et}$. This may be compared with the values of T in the models.

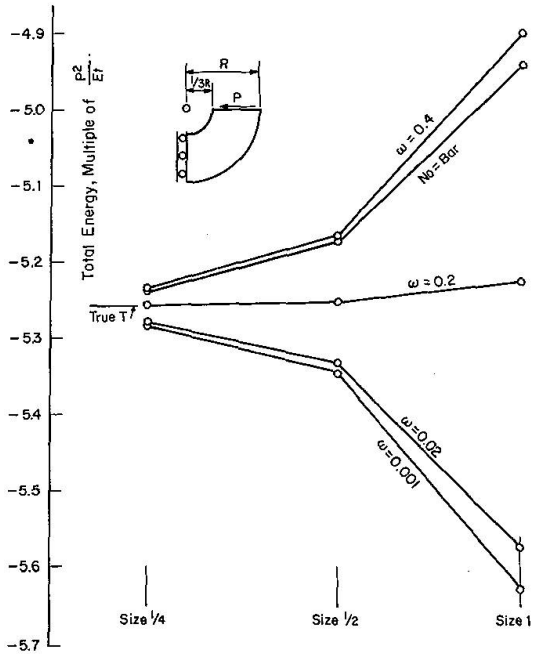

Fig. 17

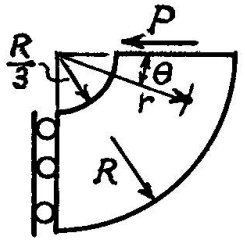

Table 6. Models of 90° Sector Plate, $\mu = 0.2$

Precision of Nodal Displacements $\delta = c\frac{P}{Et}$ (Max. Value of $c \sim 10$)

		#1. 15 Cell Model.					#2. 60 Cell Model.					#3. 240 Cell Model.				
		ω= 0.001	ω= 0.02	ω= 0.2	ω= 0.4	No-Bar	ω= 0.001	ω= 0.02	ω= 0.2	ω= 0.4	No-Bar	ω= 0.001	ω= 0.02	ω= 0.2	ω= 0.4	No-Bar
Energy T, Multiple of $\frac{P^2}{Et}$		−5.625	−5.573	−5.225	−4.898	−4.945	−5.346	−5.333	−5.252	−5.164	−5.172	−5.285	−5.280	−5.259	−5.236	−5.237
Radial Displacements.	Max. Error in c	1.76	0.778	0.279	0.865	0.594	0.526	0.197	0.082	0.238	0.254	0.085	0.050	0.022	0.062	0.071
	% of Nodes with Error $\leqslant 2\%$ in Model #1	9%	13%	48%	0%	4.3%										
	Error $\leqslant 1\%$ Mod's #2 and 3						17%	22%	62%	5%	12%	33%	85%	84%	76%	93%
Tangential Displacements.	Max. Error in c	1.48	0.534	0.163	0.925	0.364	0.46	0.144	0.047	0.250	0.102	0.069	0.045	0.009	0.061	0.027
	% of Nodes with Error $\leqslant 2\%$ in Model #1	10%	10%	60%	0%	20%										
	Error $\leqslant 1\%$ Mod's #2 and 3						10%	10%	75%	11%	37%	36%	97%	95%	91%	74%

Table 7. Models of 90° Sector Plate, $\mu = 0.2$.
Comparative Precision of Displacements in Pairs of Models
% of More Precise Displacements in Pairs of Models.

	#1. 15 Cell Model.					#2. 60 Cell Model.					#3. 240 Cell Model.				
	$\omega =$ 0.001	$\omega =$ 0.02	$\omega =$ 0.2	$\omega =$ 0.4	No-Bar	$\omega =$ 0.001	$\omega =$ 0.02	$\omega =$ 0.2	$\omega =$ 0.4	No-Bar	$\omega =$ 0.001	$\omega =$ 0.02	$\omega =$ 0.2	$\omega =$ 0.4	No-Bar
Radial Displacements			65%		35%			83%		17%			74%		26%
		26%	74%				37%	63%				24%	76%		
	9%	91%				20%	80%				24%	76%			
			91%	9%				87%	13%				84%	16%	
				9%	91%				8%	92%				18%	82%
Tangential Displacements			80%		20%			67%		33%			94%		6%
		25%	75%				23%	77%				8%	92%		
	15%	85%				13%	87%				33%	67%			
			95%	5%				87%	13%				93%	7%	
				55%	45%				53%	47%				57%	43%

In Table 7 several pairs of solutions, such as the ones with the bar cells involving $\omega = 0.001$ and $\omega = 0.02$, are compared on the basis of percentages of nodes, at which the displacements in one solution are better than in the other, and vice versa, irrespective of how great the differences are numerically.

Examination of results in Tables 6 and 7 leads to the following conclusions.

1. The total energies T in all models are quite close to the exact value in the sector $-5.2603 \frac{P^2}{Et}$. In the models having cells with $\omega = 0.001$ and 0.02, they are numerically greater than the true T (i.e. algebraically smaller), and in the other three types of cells – numerically smaller. In the cells with $\omega = 0.2$ the value of T comes very close to the true one. As the 15 cells in the coarse models are subdivided into 60 and 240 cells, their energies T change monotonically towards the true value.
2. Precision of nodal displacements in the bar cell models with $\omega = 0.2$, whose T values are the closest to the exact, is by far the best, as judged by most of the criteria in Tables 6 and 7. This applies equally well to the coarse and the fine cell models.
3. Displacement precision of all models in all ways of description improves substantially, as the number of cells increases.
4. Results with models of $\omega = 0.02$ and the no-bar cells come next in precision to those with $\omega = 0.2$. In some ways of measurement the former are better, and in the others – the latter. Farther behind them are the models with cells of $\omega = 0.001$ and $\omega = 0.4$.
5. The shape of convergence lines of the energies T on subdivision of cells (Fig. 17) is very significant. Three of these lines descend, as the cells are subdivided to ½ and ¼ sizes, and two ascend on the way to the exact value of T. Models with the best type of cells ($\omega = 0.2$) have the flattest convergence line, because their values of T are the closest to the exact.

6. Confirming the theoretical conclusion reached earlier, convergence lines of models constructed of different types of cells, do not intersect on the way to the true value of T, as the cells are subdivided.
7. The advantage of cells with a variable parameter ω lies in availability of the type of cell most suitable to the problem in question, having precision in mind. If one kind of cell in the model results in an ascending convergence line, and another – in descending, the cell, characterized by the best T, must lie somewhere in between. To obtain a comparable precision with models constructed of no-bar cells, their size must be made very fine, and the computer solution lengthy.

Notation

A	without and with subscripts and superscripts, – bar areas.
E	modulus of elasticity.
$[K]$, $[K_o]$	stiffness matrix of cell in x, y and r, t coordinates respectively.
$[L]$	transformation matrix.
P	acting load; with number subscripts, – fractions of it.
R	radius of plate.
T	total energy.
U	energy of deformation.
V	potential energy.
X, Y	with and without subscripts, – corner forces in cell.
X, Y	with subscripts and superscripts, – terms of stiffness matrix.
a_1, a_2	lengths of parallel bases of trapezoidal cell.
c	coefficient in expression for nodal displacement.
h	height of cell.
k, k_1	ratios describing the shape of cell.
n	number of circumferential rows of cells in model.
r	polar coordinate, radius.
r, t	structure coordinate axes.
t	plate thickness.
u, v	with and without subscripts, – nodal displacements.
u_o, v_o	remaining distances in Fig. 12.
x, y	cell coordinate axes.
α	base angle in the cell.
γ_{xy}	unit shear strain.
δ	nodal displacement.
ε_x, ε_y	normal unit strains.
η	a parameter.
θ	polar coordinate; angle of bar A_3 with horizontal.
μ	Poisson's ratio.
r, ω	parameters.
$\tau_{r\theta}$	shear stress.
φ	angle subtended by cell.

Acknowledgment

The research forming the basis of this work was conducted with financial assistance of the National Research Council of Canada, and this is gratefully acknowledged. The authors are also thankful to S.L. Lipson, the Head of the Department of Civil Engineering and A.G. Fowler, the Associate Director of the Computer Centre, of the University of British Columbia, for provision of computer facilities. Thanks are also expressed to the former graduate students in the Department of Civil Engineering, H.G. Charania, C.I. Mathew and Rajan Sen for some of the computer work.

Application with the view to safety and economy

With introduction of digital computer the method of Finite Element has brought into engineering practice a reliable numerical procedure for solution of numerous, hitherto insoluble, problems of practical importance, related to analyses of stresses, vibrations and instability of structures composed of continuous elastic material. Among the applications may be mentioned tall buildings depending for their strength and stability on shear walls, coverings of large areas by shells of spherical, cylindrical and other shapes and elements of modern aircraft.

In each case the structure under investigation is replaced by a model composed of an assembly of polygonal units, called finite elements or cells, of repeated pattern, planar in shape (usually rectangular, trapezoidal or triangular) or three dimensional. Planar cells may be capable of resisting stresses lying in their planes only, or flexural stresses, or both planar and flexural.

The displacements and stresses found by the computer are approximate, and their precision depends on the fineness of subdivision and the type of cells. Models made of fine cells in general give better results, but require longer computer time, and their precision may suffer from too great a number of simultaneous equations and the resultant unfavourable effect of rounding off errors by the computer, requiring special procedures for counteracting them.

Some finite elements are better than others, and the unfavourable effects mentioned here may be less pronounced, even with coarser cells. Cells may be of bar or no-bar types.

As the model is repeatedly subdivided into smaller units of the same shape and type, the solution, in all its aspects, i.e., in displacements, stresses and the energy of the system, converges gradually to the true values. Better cells are the ones, whose lines of such convergence are quite flat, i.e., whose energy, even in a coarse model, is not far from the true one.

The advantage of the cell proposed in this work lies in provision of a variable parameter, whose better value for the particular problem is found by trial to make the energy convergence line fairly flat.

The cells used in the present study are of the bar type, in the shape of equilateral trapezoid, and are suitable for solving plane stress or plane strain problems in a body, whose geometry may be described conveniently in polar

coordinates. Among suitable examples may be mentioned plane stress in a plate with a circular hole and stress analysis in rock around a circular tunnel.

Rectangle is a special case of trapezoid, and so the theory proposed here may be extended to rectangles.

The application of the theory is demonstrated on an example, whose exact theoretical solution is available.

References

1. CHARANIA, H.G.: Plane Stress Analysis with Isosceles Trapezoidal Bar Cells. Thesis for the Degree of Master of Applied Science in Civil Engineering, the University of British Columbia, Canada, 1968.
2. HRENNIKOFF, A.: Framework Method and its Technique for Solving Plane Stress Problems. Publications, International Association for Bridge and Structural Engineering, Vol. 9, 1949.
3. HRENNIKOFF, A.: The Finite Element Method in Application to Plane Stress. Publications, International Association for Bridge and Structural Engineering, Vol. 28-II, 1968.
4. HRENNIKOFF, A., and AGRAWAL, K.M.: Superior Rectangular Bar Cells in Plane Stress. Conference on "Symmetry, Similarity and Group-Theoretic Methods in Mechanics", the University of Calgary, Alberta, Canada, August 1974.
5. TIMOSHENKO, S.: Theory of Elasticity. McGraw Hill Book Co. Inc., New York, 1934.

Summary

Finite elements in the shape of isosceles trapezoids, formed of several elastic bars are proposed for analysis of plates in plane stress, when the plate geometry can be conveniently described in polar coordinates. The elements used are endowed with some distinctive features and possess a variable parameter contributing to precision of results. Stiffness matrix of the cell is derived, and the application is demonstrated on analysis of displacements of a plate in the shape of a circular sector with central cut-out, whose theoretical solution is available.

Comparison with the theoretical results shows the superiority of the proposed cell over the no-bar cell. A method for selection of a proper value for the variable parameter is suggested.

Résumé

On propose d'utiliser des éléments finis en forme de trapèzes isocèles de plusieurs barres élastiques, afin d'étudier des plaques chargées dans leur plan, lorsqu'il est indiqué de décrire la géométrie de la plaque par des coordonnées polaires. Les éléments employés sont dotés de certaines propriétés caractéristiques pour améliorer la précision. On obtient la matrice de rigidité de l'élément et on applique cette théorie à l'étude des déplacements d'une plaque en forme de secteur circulaire avec évidement central, dont la solution théorique est connue.

La comparaison entre les résultats théoriques et ceux obtenus par l'utilisation d'éléments sans barres montre la supériorité de la cellule proposée par rapport à la cellule sans barres. On propose une méthode de sélection d'une valeur propre pour le paramètre variable.

Zusammenfassung

Finite Elemente in Form isoceler Trapezoide, bestehend aus mehreren elastischen Stäben, werden für die Berechnung in ihrer Ebene belasteter Platten vorgeschlagen, wenn sich die Plattengeometrie in Polarkoordianten zweckdienlich ausdrücken lässt. Die verwendeten Elemente besitzen gewisse unterschiedliche Merkmale und einen veränderlichen Parameter, der zur Genauigkeit der Resultate beiträgt. Für die Zelle wird die Steifigkeitsmatrix abgeleitet und ihre Anwendung beim Berechnen der Verschiebung einer Platte in Form eines Kreissektors mit zentrischem Ausschnitt gezeigt, dessen theoretische Lösung verfügbar ist.

Vergleiche mit den theoretischen Resultaten zeigen die Vorzüge der vorgeschlagene Zelle gegenüber der stablosen Zelle. Es wird eine Methode zur Auswahl eines Eigenwertes für en veränderlichen Parameter vorgeschlagen.

Leere Seite
Blank page
Page vide